Design and Analysis of a Double Composite Truss Girder for Long Span Bridges Using Perfobond Leiste

Jaafar J. Saleem
Civil Engineering Department, Faculty of Engineering, Istanbul Gedik University, Istanbul, Turkiye
jaafar.alhaidari21@yahoo.com (corresponding author)

Redvan Ghasemlounia
Civil Engineering Department, Faculty of Engineering, Istanbul Gedik University, Istanbul, Turkiye
redvan.ghasemlounia@gedik.edu.tr

Haitham H. Muteb
Civil Engineering Department, Faculty of Engineering, Babylon University, Babylon, Iraq
eng.haitham.hassan@uobabylon.edu.iq

Received: 20 March 2025 | Revised: 24 April 2025 | Accepted: 27 April 2025

 DOI: https://doi.org/10.48084/etasr.11063

ABSTRACT

This research investigates the behavior and analyzes the response of a Double Composite Truss Girder (DCTG) under increasing static load, in comparison to a Single Composite Truss Girder (SCTG) under the same conditions. The benefits of a composite structure are demonstrated, namely its ability to produce a lightweight girder suitable for bridge superstructures, especially in long continuous spans with the idea of converting the concrete web to steel truss. The present study also aims to increase the girder's ability to resist high hogging moments in the negative moment regions. The experimental work involved the fabrication and testing of eight composite truss girder specimens with constant dimensions of 2620 mm x 350 mm x 400 mm of steel warren truss girder under two-point static load. A validation study was conducted using numerical analysis methods along with the Abaqus software program to simulate the eight models. Perfobond Leiste (PRL) shear connectors were deployed and the slip ratio, deflection ratio, girder strength, and stress–strain relationship results for each sample were presented.

Keywords--perfobond lieste shear connector; double composite girder; experiment study; Abaqus simulation; hogging moment; warren truss; static load

I. INTRODUCTION

Given their high durability and quick construction time, steel-concrete composite girders are frequently utilized in structural constructions. A composite element is defined as the combination of two or more materials joined in a specific manner to simultaneously utilize the beneficial properties of each material. The structural stiffness and load-carrying capacity increase because steel and concrete have different, complementary characteristics [1]. The quality and behavior of these two composite elements depend on the quality of the shear connector regarding geometry and the process of shear force flow transfer [2]. When flexural strength and stiffness increase, longer spans and shallower beam depths can be achieved, while it is possible for a faster, more convenient, and more economical construction to be accomplished [3]. The main objective of having shear connectors is to achieve an optimal interaction between the concrete structure and the steel components, or any other two materials, which require very high stress resistance to prevent any failure due to creep or separation of each element [4]. Several types of shear connectors are used to connect two elements, thereby increasing moment resistance by enhancing the moment of inertia of the composite section. Among these, PRL connectors are considered the most common due to their effective load transfer mechanism, offering excellent shear resistance, high load-bearing capacity, and a large bonding area. They are particularly suitable for applications requiring high shear resistance, especially in bridge structures [1]. A typical PRL shear connector consist of a steel plate containing several holes, where several steel bars are passed through these holes to increase the structural bonding between the steel and concrete elements [2]. Advanced computer programs are used for detailed simulations of shear connector behavior under different loading conditions. These tools make it possible to model the design of the shear connector and all composite

parameters, including applied loads, to predict performance without the need for extensive physical testing [2]. Composite steel girder provides greater efficiency and certified results, especially for bridges with long spans, around 60 to120 m, and over 120 m for the very long span bridge, meeting the seismic requirement factor in their designs [5].

In [6], an experimental study was conducted to investigate the performance of composite girders under hogging moments using different types of shear connectors, such as shear studs and PRL, when subjected to maximum applied loads. Authors in [7] examined the gradual deterioration of stud shear connections through numerical analyses, focusing on the residual static performance and remaining fatigue lifespan of post-tensioned steel-concrete composite beams. The results demonstrated the impact of stud failure on the shear stress at the beam ends where the stud fracture occurred. Authors in [8] introduced a novel Steel-Concrete Composite Link Slab (SCC-LS) and conducted a full-scale Finite Element (FE) simulation to evaluate its mechanical performance, which was also analyzed through theoretical calculations. It was observed that increasing the thickness of the steel plate significantly reduced the tensile stress on the concrete surface. Authors in [9] examined the shear behavior of composite connections by push-out experiments involving various shear connectors, supported by theoretical and numerical studies. The results indicated a distinction in the failure mechanisms among the different types of shear connectors. Authors in [10] used a type of truss composite girder to verify the shear performance of composite girders. Based on the crack indicators and observed failure modes, the behavioral characteristics of the composite girder were obtained from two specimens. Authors in [11] applied Finite Element Analysis (FEA) to a steel-concrete composite plate resting on the axial bar using a four-node quadrilateral FE for a steel-concrete composite plate combined with a truss element. They used a numerical example demonstrating a very small difference between the current study and the SAP2000 results.

Authors in [12] examined of the rotation capacity for hogging and sagging regions in continuous composite beams to determine the ultimate strength deploying the plastic design theory. Authors in [13], whose research is closely related to the present work thesis, introduced a new type of composite tubular truss bridge and provided the detailed specifications of its design. The bridge superstructure consists of a double composite section, composed of rectangular tubular chords filled with concrete and a prestressed concrete slab. The results revealed that the joint with the PBR design achieves approximately 22% higher punching shear resistance compared to the joint without PBR, indicating that PBR significantly enhances the performance of concrete. Authors in [14] analyzed composite cellular beams with hogging moment loading based on elastic and inelastic behavior. ABAQUS software was used to perform the finite element analysis (FEA) in this study. The results of the study showed that the composite steel-concrete member and the hogging moment region are prone to multiple types of failures.

II. STUDY OBJECTIVES

The main objectives of this study are:

- To determine the dimensional properties of the PRL by conducting push-out tests on three individual samples. The results will provide insights into the shear connectors' behavior and contribute to the final design of the PRL in the main composite girder samples.
- To show the effectiveness of the variables of shear connector length, thickness, and plate holes on the load-relative slip ratio and the interface uplifts.
- To explain the composite bond, which refers to the ductility of the shear connectors. This describes their ability to undergo significant plastic deformation before failure and indicates how much the shear connector can deform without losing its capacity to transfer shear forces between the steel elements and the concrete deck in a composite structure.
- To show the effectiveness of DCTG in the hogging moment value and crack resistance compared to the SCTG at the mid supports.
- To show the effectiveness of DCTG in the deflection ratio at the sagging regions, which are affected by the positive moments.
- To analyze all continuous girder samples according to modes of failure and strength capacity.

III. EXPERIMENTAL WORK

A. Specimen Design and Fabrications

This research consisted of two categories of tested specimens: SCTG and DCTG. Overall, eight composite steel truss girders were cast and four specimens were examined for each category, with different dimensions and thicknesses for the concrete and perfobond rib shear connector. A range of thicknesses was used for the steel flange and the vertical and diagonal truss member with a 45^{o} angle. Figures 1-3 and Tables I-IV illustrate the specimens' details and dimensions.

TABLE I. DETAILS OF THE SPECIMENS (SCTG AND DCTG)

Model	Length (mm)	Top flange thickness (mm)	Bottom flange thickness (mm)	Deck slab thickness (mm)	Concrete strength (MPa)
SCTG-1 DCTG-1	2620	6	6	70	35
SCTG-2 DCTG-2	2620	8	8	80	35
SCTG-3 DCTG-3	2620	10	10	90	35
SCTG-4 DCTG-4	2620	12	12	100	35

The SCTG is connected only at the top, while DCTG is connected at both the top and bottom. In both categories, the top steel flange is connected to the concrete deck slab using shear connectors. The plates were cut using a laser cutting machine. The vertical and diagonal steel members were formed as a steel frame made from Hollow Structural Sections (HSS) steel tubes. All members were connected to the flanges by MIG welding with a 4 mm thickness, using a shielding gas mixture of 75% argon and 25% CO_2.

TABLE II. DETAILS OF THE PRL FOR SCTG AND DCTG

Model	Height (mm)	Ribs plate thickness (mm)	Hole Diameter (mm)	Hole spacing (mm)	Reinforcement bar diameter (mm)
SCTG-1 DCTG-1	40	2	20	50	6
SCTG-2 DCTG-2	50	4	25	60	10
SCTG-3 DCTG-3	60	6	30	70	12
SCTG-4 DCTG-4	70	8	35	80	16

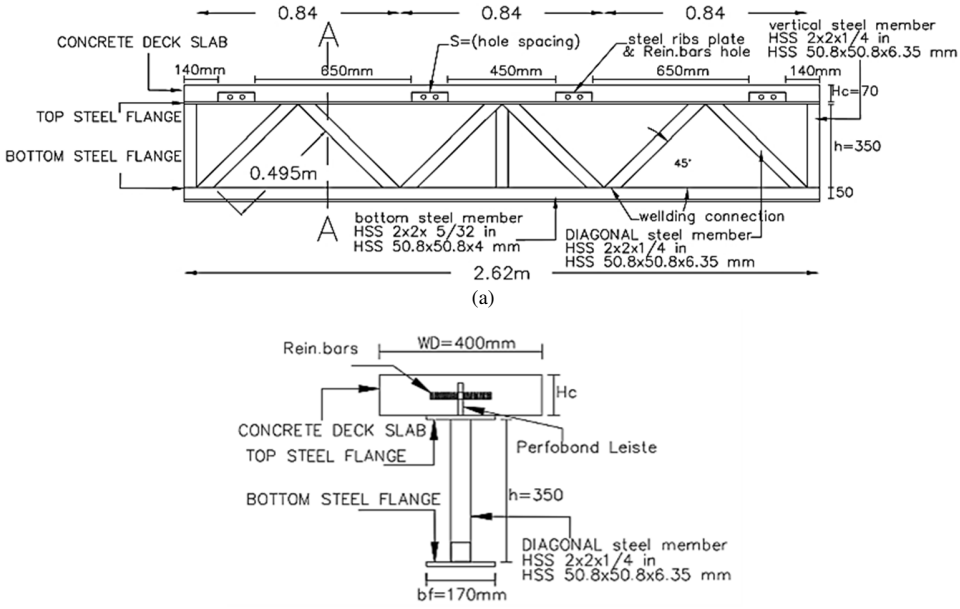

Fig. 1. SCTG models. (a) Layout of specimen, (b) section view (A-A).

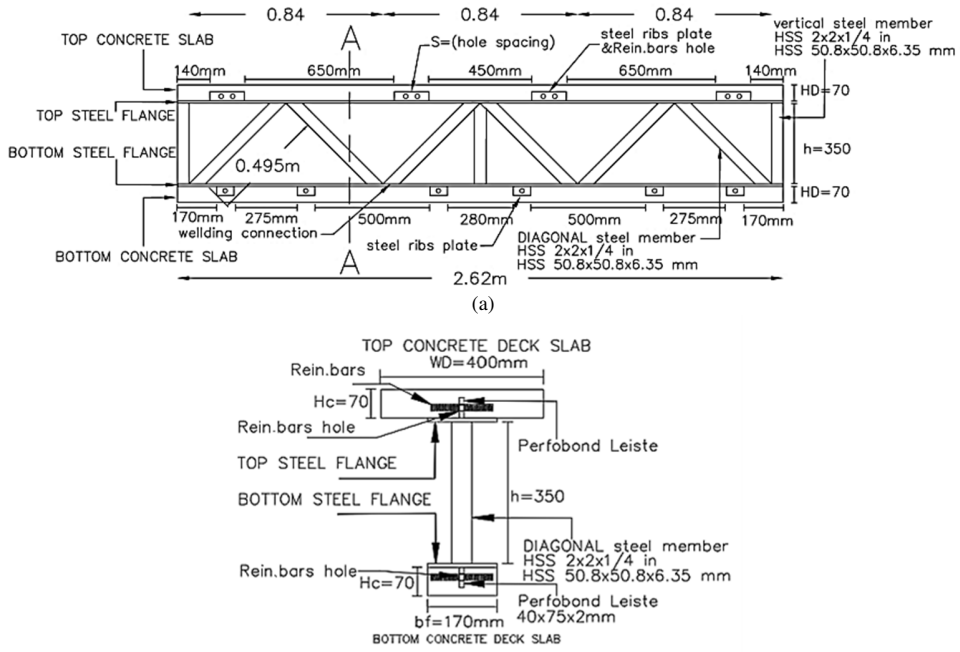

Fig. 2. DCTG models. (a) Layout of specimen, (b) section view (A-A).

The PRL shear connectors were welded to both the top and bottom steel flanges. The hole in the steel plate is made by a drilling machine with the required diameter. This category consists of deck slab made from reinforcement concrete (35 MPa) pouring with an effective width of 400 mm and differing in depth from one specimen to another. Both concrete slabs were reinforced with 6 mm steel bars placed in both the longitudinal and lateral directions. Figures 3-8 illustrate the manufacturing, concrete pouring, and casting steps. A total of eight molds were used in the testing of the main composite truss girders covering the top concrete and bottom flanges, specifically for the DCTG specimens.

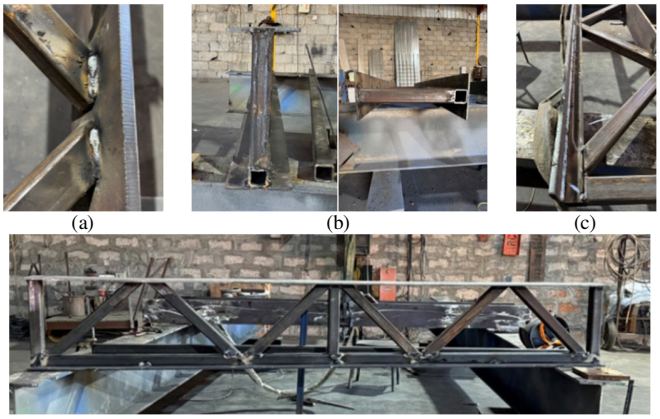

(a) (b) (c) (d)

Fig. 3. SCTG steel frame: (a) HSS diagonal member welding, (b) cross-section of the truss girder, (c) welding stage of the bottom HSS, (d) side view of the truss girder (steel plate with vertical and diagonal HSS).

(a) (b) (c)

Fig. 4. SCTG PRL implementation: (a) steel plate cutting machine, (b) PRL and hole bars welding, (c) shear connector final shape.

B. Measurement Equipment

Foil strain gauges are used to measure the relative changes in a material's length, occuring because of the application of forces. Six foil strain gauges with a resistance of 120 ohms and a Gauge Factor (GF) of 2 were used. Strain gauges of type FLA-10-11 were applied to measure strain in the steel components, while PL-60-11 gauges were used on the top and bottom surfaces of the concrete deck slab for each specimen. Figure 9 shows the strain sensor positions. Two Linear Variable Differential Transformer (LVDT) indicators are used in the bottom specimen in the middle distance to give the deflection profile. To measure the relative slip ratio of the composite structure, two LVDT devices were installed at the top of both SCTG and DCTG, positioned between the upper steel flange and the upper concrete surface on the outer face. This setup was used to monitor the movement at the interaction interface, which depends on the type of PRL, as illustrated in Figure 10.

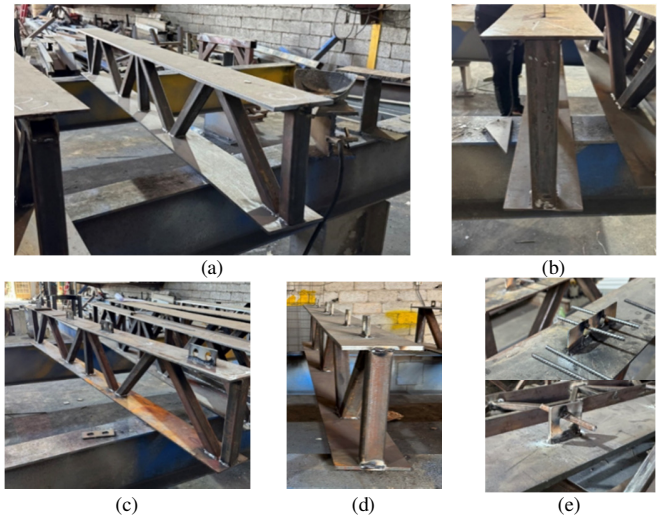

(a) (b) (c) (d) (e)

Fig. 5. DCTG steel frame: (a) steel frame side view, (b) steel cross-section, (c) top PRL shear connector, (d) bottom PRL shear connector, (e) shear connector final shape.

Fig. 6. Final manufacturing stage of DCTG and SCTG.

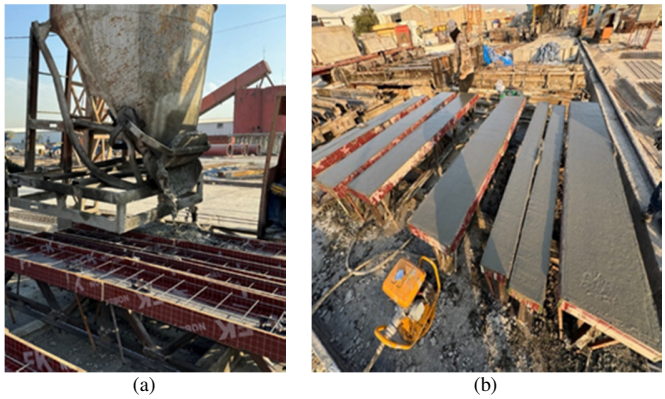

(a) (b)

Fig. 7. Steps of concrete pouring for SCTG and DCTG: (a) pouring stage of the concrete mix, (b) final stage after casting the top and bottom concrete deck slabs.

(a) (b)

Fig. 8. Concrete casting of the main truss girder: (a) concrete casting stage of SCTG, (b) concrete casting stage of DCTG.

(a) (b) (c)

Fig. 9. Position of the strain gauges: (a) installation of the strain gauge on top concrete, (b) strain gauge on bottom steel, (c) installation of the strain gauge on bottom concrete deck slabs.

(a) (b)

Fig. 10. Position of the LVDT devices: (a) relative slip recording, (b) deflection recording.

C. Loading Methodology

The main loading test of the eight composite truss girders was conducted on-site under a special agreement, using a loading device with a capacity of 250 tons. The specimen was installed on three supports—two at both ends and one at the midspan. A static load was applied at two points between the central support and the edge supports, generating a negative moment at the support regions and a positive moment at midspan. By using the two hydraulic jacks of 3000 kN load capacity, each jack can apply load on the specimen till failure mode occurs, as shown in Figures 11 and 12.

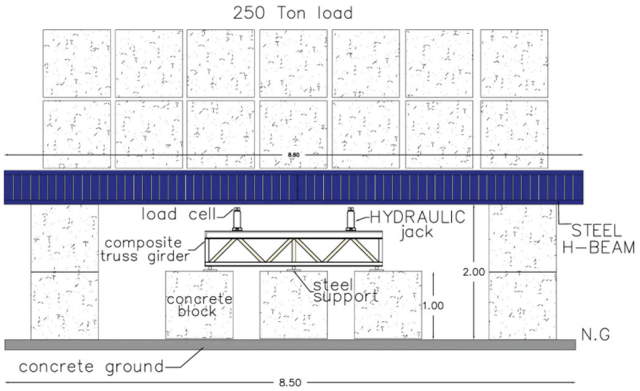

Fig. 11. The hydraulic machine and load system design sheet.

(a) (b)

Fig. 12. Loading methodology: (a) system installation, (b) test situation with hydraulic jack over the specimen and all the sensor devices connected to the data logger.

IV. NUMERICAL ANALYSIS

The purpose of using ABAQUS 2023 software is its exceptional capability in analyzing plasticity and mechanical issues relevant to this research, as well as providing data on composite truss behavior.

A. Material Parameters

- The steel plate flanges behaved elastically, with a Poisson's ratio of 0.3 and a Young's modulus of 200,000 MPa.
- In the plastic stage, the steel materials are defined with yield strengths of 690 MPa, 700 MPa, and 718 MPa for reinforcement bars of 10 mm, 12 mm, and 16 mm diameter, respectively.
- The steel flanges were defined with yield strengths of 407 MPa and 520 MPa for the HSS steel truss members (vertical and diagonal), respectively, and 517 MPa for the shear connector steel plate (rib plate). These values are based on the results of the steel tensile test.
- For the concrete material, Normal Weight Concrete (NWC) was used. In the elastic stage, the Young's modulus of concrete (Ec) was defined as 2.30E+09 Pa, and the Poisson's ratio (ν) as 0.2. In the plastic stage, the Concrete Damage Plasticity (CDP) model was used, with a compressive strength of 35 MPa and tensile strength of 4.2 MPa. These parameters were obtained from laboratory material tests.

B. Assembly of Specimen Parts

In this step, the assembly is performed to ensure that all parts are properly connected. Figures 13 and 14 show the specimens after assembly for both SCTG and DCTG.

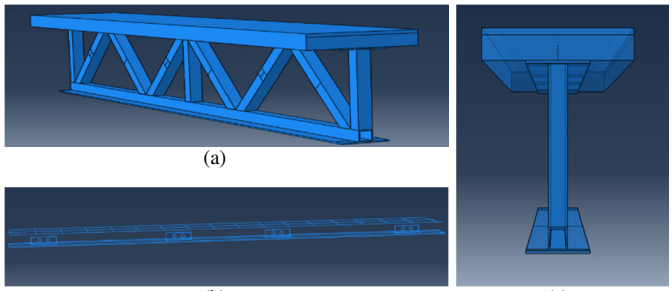

(a) (b) (c)

Fig. 13. Assembling of SCTG models: (a) 3D view of the single composite truss girder, (b) top PRL with the BRC 300 × 150X6 mm, (c) specimen front view.

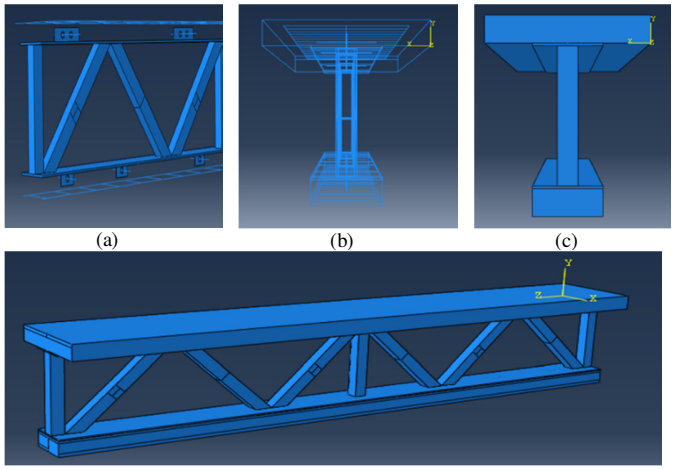

(a) (b) (c) (d)

Fig. 14. Assembly of DCTG models: (a) top and bottom PRL with BRC mesh (300 × 150 × 6 mm), (b) detailed front view of the connection, (c) front view of the double composite truss girder, (d) 3D view of the assembled double composite truss girder.

C. Part Interactions, Loading, and Boundary Conditions

To create the interaction property model between the surfaces of the specimen parts, the following steps were taken:

- Defining the contact with tangential behavior between the support (master surface, shown in red) and the bottom girder (secondary surface, shown in pink). Using the penalty friction formulation with a friction coefficient of 0.35.
- For normal behavior, defining the contact as normal hard contact, allowing separation after contact when pressure is applied.
- Defining surface-to-surface contact between the concrete surface and the steel flange surface of the truss frame, simulating normal contact behavior.
- A tie constraint was used to connect the steel flanges and the shear connector ribs. The steel flange surface was treated as the master surface, while the steel ribs (shear connectors) and concrete were considered the slave (secondary) surfaces.
- An embedded region constraint was used to model the connection between the BRC reinforcement bars and the concrete, as well as between the PRL rib shear connectors and the concrete through the hole rebars, as portrayed in Figures 15 and 16.

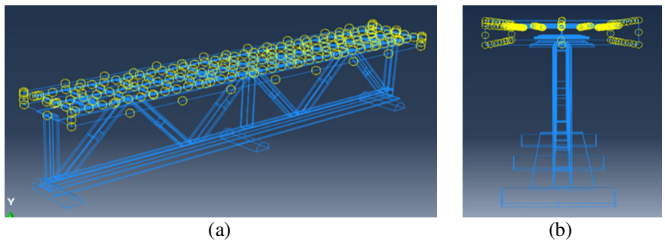

(a) (b)

Fig. 15. Embedded region constraint applied to the top concrete in the SCTG model: (a) side view, (b) front view.

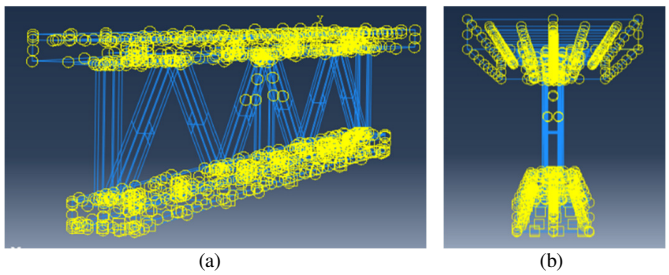

(a) (b)

Fig. 16. Embedded region constraint applied to the top concrete in the DCTG model: (a) side view, (b) front view.

Loading was applied as concentrated forces on the surface of the concrete slab of the composite girder, using two loading points (RP.4 and RP.5), each subjected to a maximum load of 50 tons. To ensure uniform load distribution, constraint couplings were defined as structural distributions, bonding the reference points across the width of the concrete part. The boundary condition is essential for defining how the model interacts with its surrounding environment. The movement of nodes in the finite element model was restricted to ensure that the specimen simulation accurately represents real world boundary conditions and constraints, as illustrated in Figure 17.

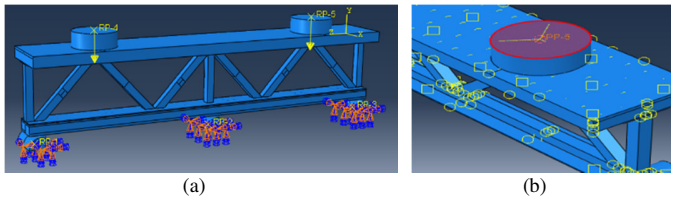

(a) (b)

Fig. 17. Loading location and boundary condition: (a) modeling of the applied static load and modeling of the support boundary condition, (b) coupling constrain load distribution of RP-4 and RP-5.

D. Model Meshing and Elements Selections

Meshing is defined as the division of the sample into very small parts, which is an important step in any FEA. In this study, the meshing is performed using 25 mm size elements to achieve accurate results from the shell and solid element. The elements selected for analysis are:

- The S3R triangular shell element to mesh the steel truss HSS members, employing traditional reduced integration.
- The C3D8I element was used to mesh rectangular mesh the concrete deck slab, shear connector palate, and steel flange.
- The T3D2 linear truss element was used to mesh the steel reinforcement rebars.

For the PRL rib shear connector, it is important to modify meshing by deploying the medial axis technique to achieve better mesh quality, especially for cylindrical geometries. Figures 18, 19 illustrate the model meshing for the SCTG and DCTG specimens.

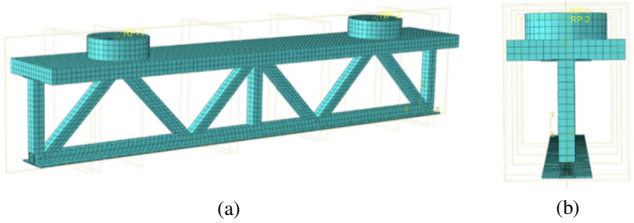

(a) (b)

Fig. 18. Entire meshing of SCTG: (a) model side view, (b) model front view.

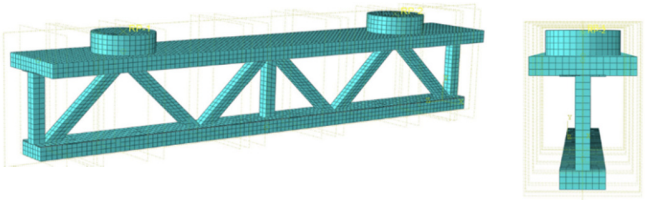

(a) (b)

Fig. 19. Entire meshing of DCTG: (a) model side view, (b) model front view.

V. RESULTS AND ANALYSIS

A. Modes of Failure and Girder Strength

The shape of failure that occurs for SCTG samples shows severe cracks at the top concrete under the hydraulic jack location due to the applied load. The main failure was located at the bottom HSS steel member and steel flange near the edge support. Failure also occurred at the midsection of the HSS steel member due to high compression, as shown in Figure 20. The strength of girders was 65 tons for SCTG-1 and SCTG-2, and 52 tons and 50 tons for SCTG-3 and SCTG-4, respectively. For the DCTG samples, the results show an advanced failure occurring at the bottom concrete deck slab near the steel flange, caused by high compressive stresses generated by shear forces acting on the section. Additionally, concrete detachment from the PRL shear connector causes uplift of the steel flange, leading to shear connector failure in this region, as shown in Figure 21. The measured strength capacities for the DCTG specimens were 71 tons for DCTG-1, 61 tons for DCTG-2, 71 tons for DCTG-3, and 75 tons for DCTG-4.

The difference between the experimental results and numerical analysis results for SCTG-1 and SCTG-2 ranged from 3.6% to 5.1%, which is considered acceptable given the number of variables involved in the model. The difference percentage ranged from 19.4% to 25.1% for SCTG-3 and SCTG-4, as these samples experienced early damage during the experimental tests. The result validation for the DCTG samples, based on the experiment and numerical analysis, ranged between 4.7% and 14.3%. These differences are considered acceptable.

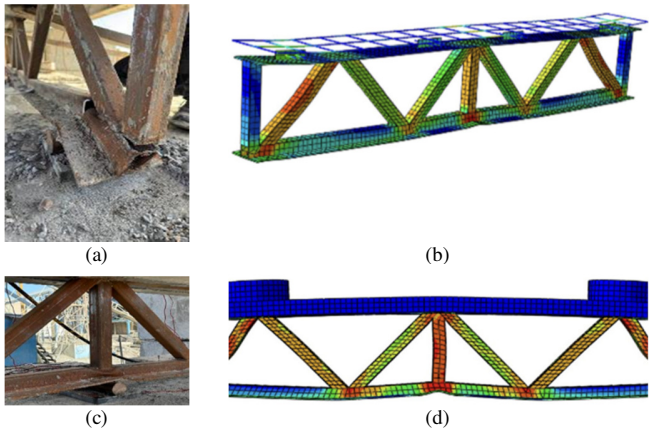

(a) (b)

(c) (d)

Fig. 20. Modes of failure and simulation results for SCTG samples: (a) site test showing damage to bottom HSS, (b) side view of stress distribution in model members, (c) site test showing damage to bottom and middle HSS, (d) validation of bottom HSS damage in specimen.

B. Stress-Strain Relationship

Strain data were recorded on the top concrete surface (maximum negative moment) using two sensors labeled S5 and S6, and at the lower steel flange (maximum positive moment) using four sensors labeled S1, S2, S3, and S4. For the SCTG samples, the results show that the four strain sensors on the steel flange exhibited different values but followed the same pattern. The bottom steel flange sensors indicated a higher elastic and plastic strain percentage compared to the very low strain percentages recorded on the top concrete slab, indicating that the upper part was exposed to a higher strain ratio (Figure 22). In contrast, for the DCTG samples, the average strain sensor readings showed greater stability and a better correlation between the applied load and strain sensor output. This contradicts with the SCTG samples, which displayed very high stress readings and greater variation at the same load levels due to unstable and uneven load distribution on the surface. The stress-strain curves illustrating these behaviors are shown in Figure 23.

C. Deflection Ratio

There is a significant increase in deflection from the initial load stage to full loading, with a particularly large and unstable deflection gap observed between the plastic load stage and full load for the SCTG samples.

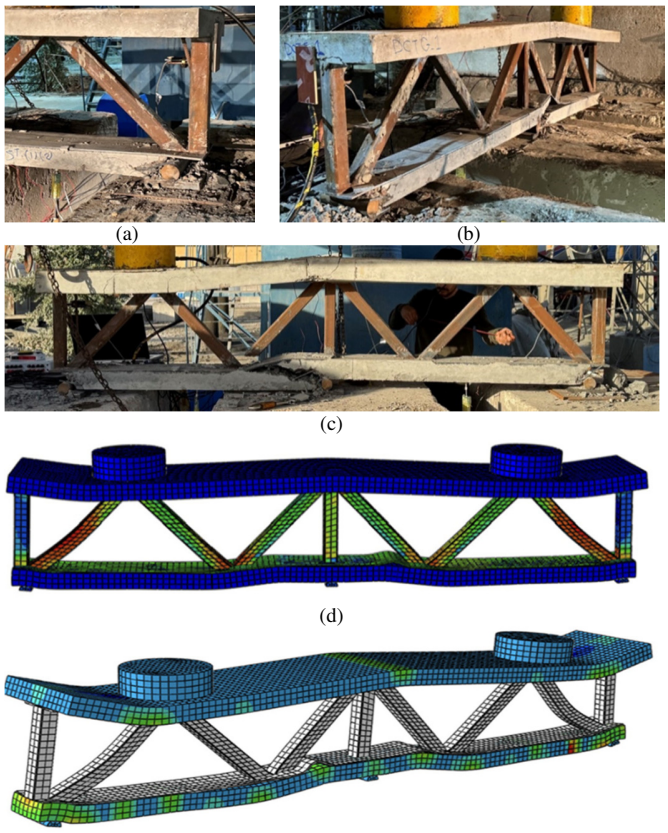

Fig. 21. Modes of failure with simulation results for DCTG samples: (a) site test showing bottom concrete deck slab damage at edge, (b) concrete damage in the bottom compression region, (c) diagonal HSS damage caused by high tensile force, (d) side view of simulated model stress distribution in members, (e) validation of specimen damage on the bottom flange due to uplift.

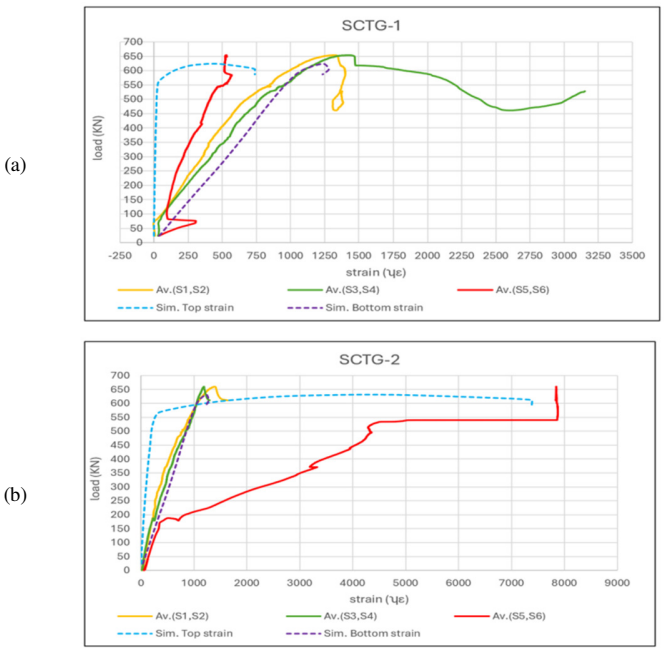

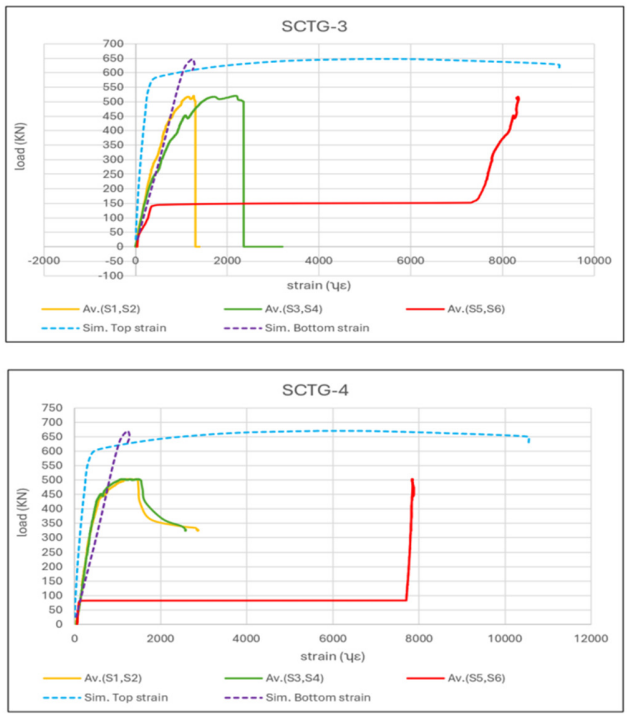

Fig. 22. Stress-strain curve for SCTG samples with the simulation results: (a) SCTG-1, (b) SCTG-2, (c) SCTG-3, (d) SCTG-4.

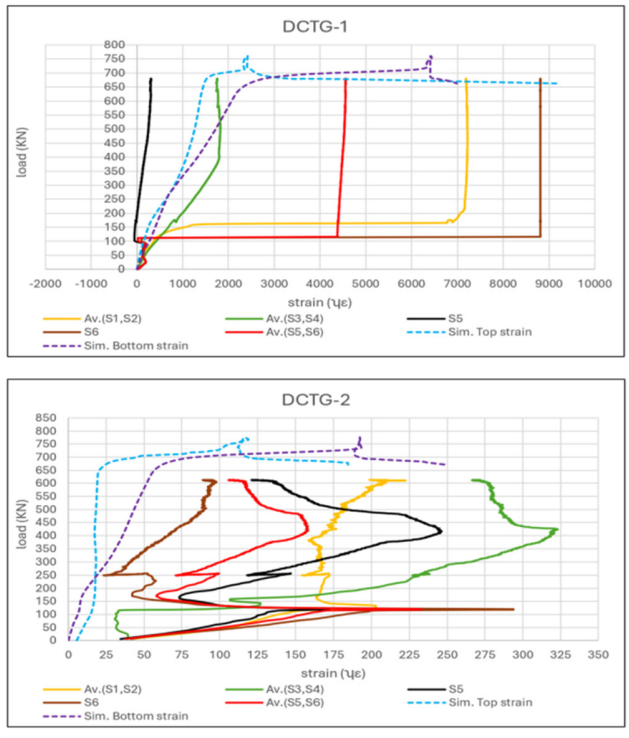

(c)

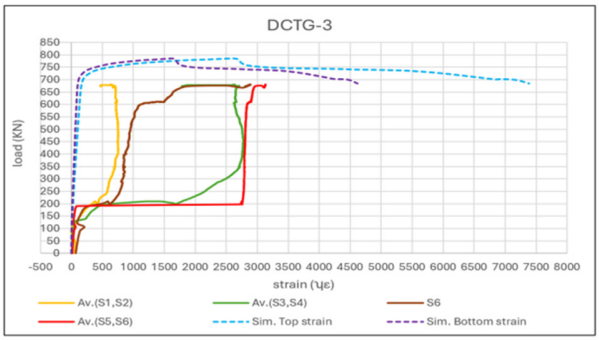

(d)

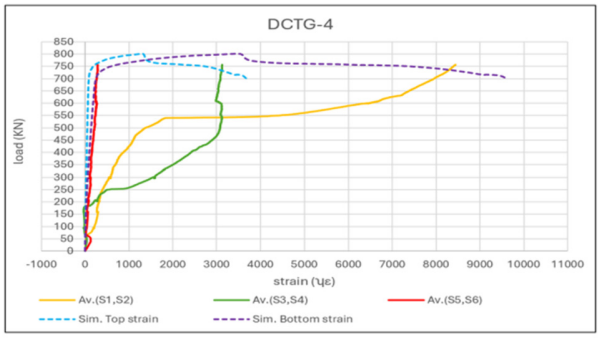

Fig. 23. Stress-strain curve for DCTG samples with the simulation results: (a) DCTG-1, (b) DCTG-2, (c) DCTG-3, (d) DCTG-4.

TABLE I. DETAILS OF THE LOAD DEFLECTION FOR SCTG

Model	Experiment results		Experiment results		Deflection discrepancy ratio %
	Ultimate load (kN)	Deflection (mm)	Ultimate load (kN)	Deflection (mm)	
SCTG-1	654	8.98	622	9.2	2.3%
SCTG-2	658	8.7	634	9.31	6.5%
SCTG-3	520	10.02	643	9.7	3.1%
SCTG-4	502	9.8	671	10.1	2.9%

(a)

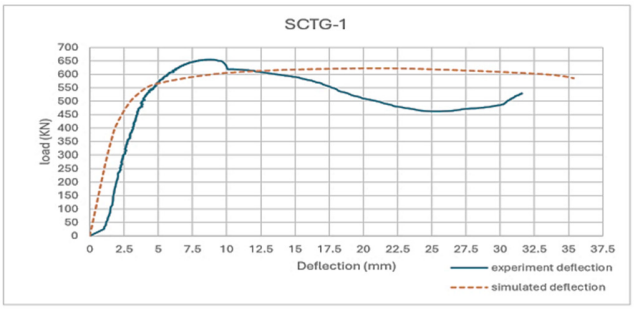

(b)

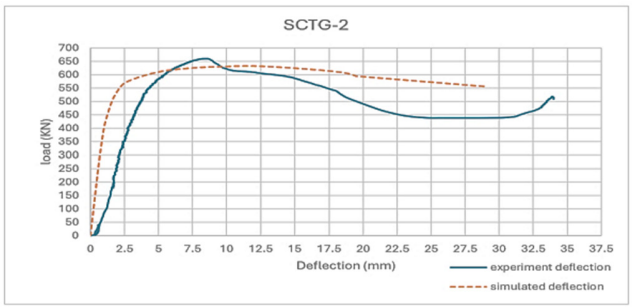

(c)

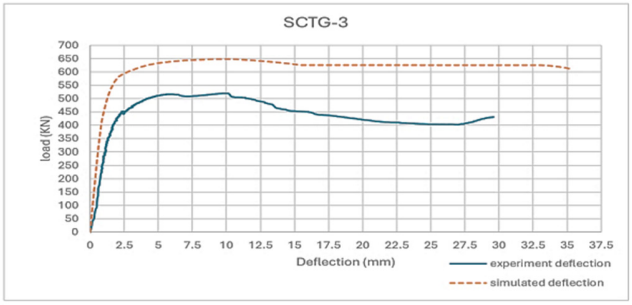

(d)

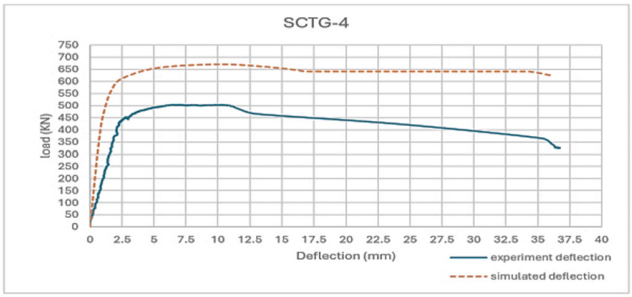

Fig. 24. Load-deflection curves for SCTG samples: (a) SCTG-1, (b) SCTG-2, (c) SCTG-3, (d) SCTG-4.

Table III and Figure 24 display a discrepancy ratio ranging from 2.3% to 6.5% between the experimental and numerical analysis results for SCTG. Meanwhile, for the DCTG samples, the deflection ratio from the initial load stage to full loading was moderate, resulting in specimens with highly stable deflection control. The assessment is considered acceptable, with a deflection discrepancy ratio ranging from 2.6% to 10.1%, as shown in Table IV and Figure 25. These deflection values are mainly affected by the thickness of the concrete and steel flanges at this category, unlike the case of the first category. The deflection gets increased after the point of fracture failure when the bond of concrete and steel is lost.

(a)

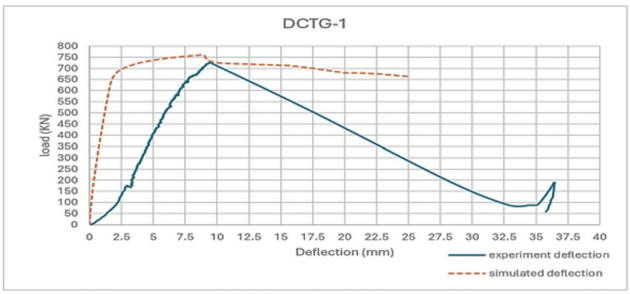

(b)

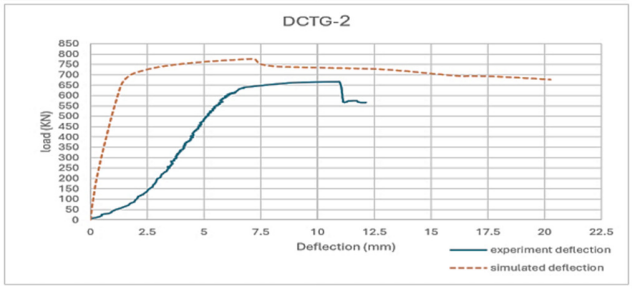

(c)

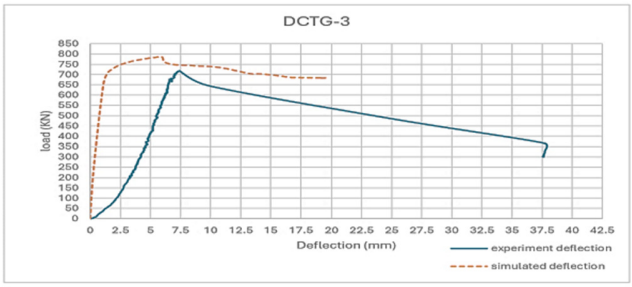

(d)

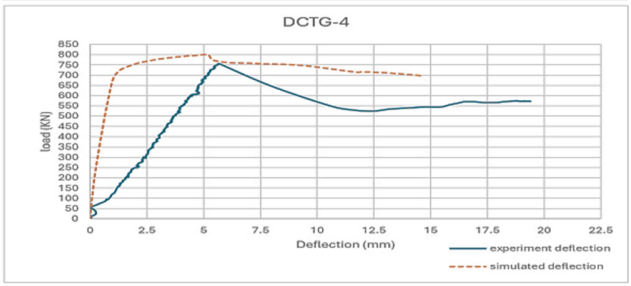

Fig. 25. Load-deflection curve for DCTG samples: (a) DCTG-1, (b) DCTG-2, (c) DCTG-3, (d) DCTG-4.

TABLE II. DETAILS OF THE LOAD DEFLECTION FOR DCTG

Model	Experiment results		Theoretical results		Deflection discrepancy ratio %
	Ultimate load (kN)	Deflection (mm)	Ultimate load (kN)	Deflection (mm)	
DCTG-1	725	7.80	761	8.21	4.9%
DCTG-2	665	7.3	776	7.11	2.6%
DCTG-3	716	6.14	785	5.88	4.2%
DCTG-4	754	4.6	801	5.12	10.1%

D. Relative Slip

The positive signs indicate that the top concrete moves inward toward the structure's center, while the steel flange moves outward; negative signs represent the opposite directions. Table V compares the simulated results with the actual slip in the experiment study for SCTG samples. A low discrepancy percentage of around 12.3-27.5% was observed, as illustrated in Figure 26. On the other hand, as shown in Table VI and Figure 28, the DCTG simulated slip results exhibit a discrepancy ranging from 6% to 22% compared to the actual measurements.

TABLE III. DETAILS OF THE LOAD-SLIP RATIO FOR SCTG.

Model	Experiment results		Experiment results		Deflection Discrepancy ratio %
	Ultimate Load (kN)	Deflection (mm)	Ultimate Load (kN)	Deflection (mm)	
SCTG-1	654	-1.38	622	1.21	12.3%
SCTG-2	659	-0.652	634	0.54	17.1%
SCTG-3	520	0.347	643	0.42	17.3%
SCTG-4	503	0.29	671	0.21	27.5%

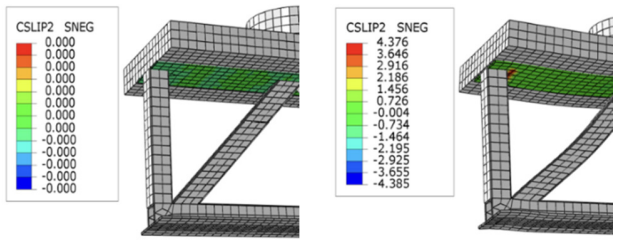

(a) (b)

Fig. 26. Slip location between top concrete and steel flange for SCTG samples: (a) before loading status, (b) full loading status.

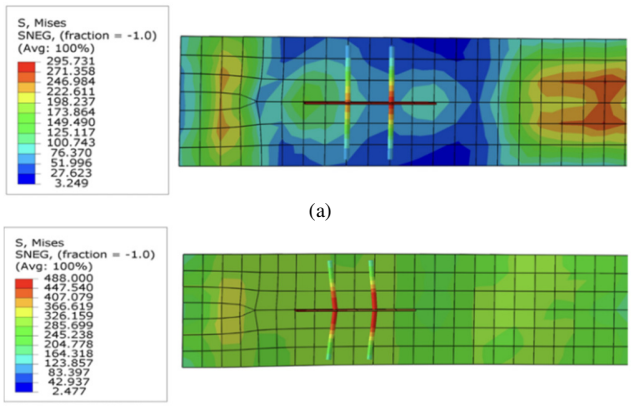

(a)

(b)

Fig. 27. PRL shear connector deformation due to slip action on the top concrete for SCTG samples: (a) PRL acting at half load, (b) PRL acting at full load.

TABLE IV. DETAILS OF THE LOAD-SLIP RATIO FOR DCTG.

Model	Experiment results		Theoretical results		Deflection discrepancy ratio %
	Ultimate load (kN)	Max. slip (mm)	Ultimate load (kN)	Max. slip (mm)	
DCTG-1	725	-1.08	761	-1.15	6%
DCTG-2	665	0.53	776	-0.64	17%
DCTG-3	717	0.28	785	-0.32	12.5%
DCTG-4	755	0.27	801	-0.21	22%

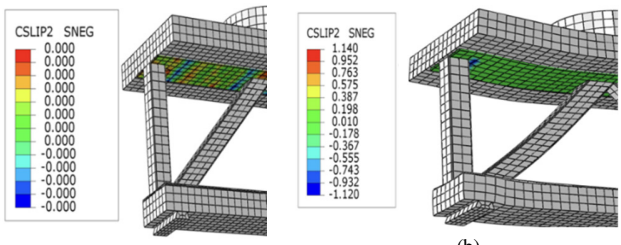

(a) (b)

Fig. 28. Slip location between top concrete and steel flange for DCTG samples: (a) before loading status, (b) full loading status.

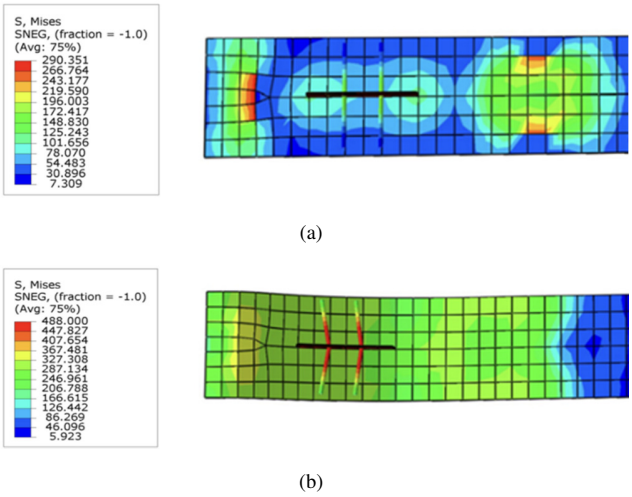

Fig. 29. PRL shear connector deformation due to slip action on the top concrete deck slab for DCTG samples: (a) PRL acting at half load, (b) PRL acting at full load.

E. Initial Cracks (Pcr) and Ultimate Cracks (Pul)

Cracks identified through visual inspection, as well as the data shown in Tables VII and VIII, include both elastic and plastic load levels. It is obvious that the initial carks appeared at the intermediate stages of loading, unlike the SCTG samples that appeared at the primary loading stage For the DCTG samples, the ultimate service cracks appeared at a much later (more advanced) loading stage, whereas for the SCTG samples, these cracks appeared between intermediate and advanced loading stages.

TABLE V. DETAILS OF THE LOAD-SLIP RATIO FOR DCTG.

Model	Ultimate load (kN)	Pcr	Pul	Remark
SCTG-1	654	205	495	H.G.R.C
SCTG-2	658	254	507	H.G.R.C
SCTG-3	520	346	471	H.G.R.C
SCTG-4	502	360	463	H.G.R.C

TABLE VI. DETAILS OF THE INITIAL AND ULTIMATE CRACKS FOR DCTG SAMPLES.

Model	Ultimate load (kN)	Pcr	Pul	Remarks
DCTG-1	725	320	661	H.M.R.C
DCTG-2	613	375	582	H.M.R.C
DCTG-3	716	473	692	H.M.R.C
DCTG-4	754	523	730	H.M.R.C

VI. CONCLUSION

Based on the results obtained from both the experimental and numerical analyses, major parameters were investigated. The proposed Finite Element Analysis (FEA) method using the ABAQUS program appears to be valid for evaluating the response of composite truss girders under static load, as indicated by the close agreement of the reaction forces. As the load gets applied on all samples, the strain sensors show lower stress values at the top concrete surface (hogging moment region) for the Double Composite Truss Girder (DCTG) than the Single Composite Truss Girder (SCTG) by 42.7%. In contrast, the bottom surface (sagging moment region) for both SCTG and DCTG was exposed to high stress values. The deflection values of DCTG were 31% less than those of SCTG. This reduction is attributed to the delayed full interaction loss between the top concrete deck slab and steel flange, due to the increased contribution of the bottom Perfobond Leiste (PRL) shear connectors. Moreover, the elastic and plastic deflection resistances for the SCTG were 79% and 95.7%, respectively. The results show an improvement for DCTG, when this deformation was at 89% and 97.1%, respectively.

In terms of load-slip ratio, the results exhibit a decrease in slip values from the first to the fourth type of PRL shear connectors by 79.2% and 75% for the SCTG and DCTG, respectively. Additionally, slip values decreased by 18.7% in DCTG compared to SCTG, demonstrating a higher ductility range. Increasing the thickness of the concrete and steel flange layers contributed to an increase in the moment of inertia of the composite girder, improving deflection resistance. Moreover, the composite feature of the DCTG specimens enhanced the deflection resistance from DCTG-1 to DCTG-4 by an average percentage of 37.6%, while it continued increasing for SCTG girders.

The load level at which elastic cracks (initial cracks) began in DCTG occurred at a higher load than in SCTG, with overall average percentages of 60% and 49% of ultimate load, respectively. This delay leads to a later onset of plastic crack deformation (ultimate cracks), increasing the girder's crack resistance by 11.1%, especially in the hogging moment regions. The results show that plastic cracks appeared at 94% and 82.9% of the ultimate load for the DCTG and SCTG, respectively. The results suggest that the strength capacity of the DCTG specimens was approximately 13% higher than that of the SCTG specimens. Specifically, the maximum bearing load capacity of the DCTG-4 girder was 75 tons, compared to 65 tons for the SCTG-4. Overall, the findings reveal that DCTG demonstrates improved performance over the single SCTG across all measured parameters, as shown in Figure 30.

Typical long continuous bridge spans experience advanced cracking in the concrete deck slab due to high hogging moments at mid-support regions. The composite feature provides significant enhancement, resulting in a more reliable and durable composite girder—especially for long continuous bridges—by effectively resisting forces generated from the bridge's self-weight and vehicular traffic. Using a steel truss system transfer loads more efficiently and also reduces self-weight compared to conventional prestressed or post-tensioned concrete girders, which may weigh hundreds of tons. The use of PRL shear connectors positively affects the girder's strength due to their ability to resist higher shear flow compared to other types of shear connectors.

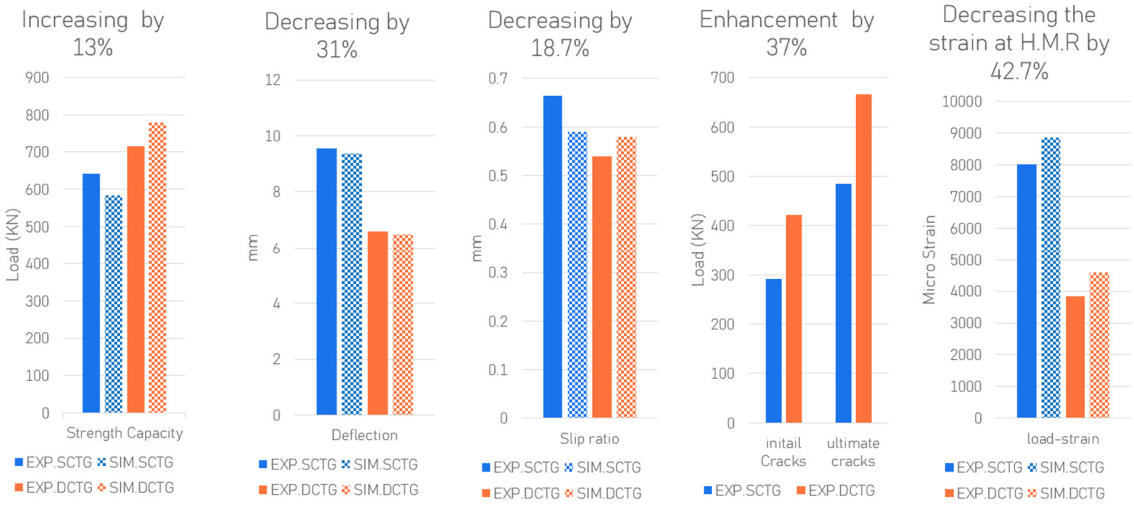

Fig. 30. Experimental (EXP) and simulated (SIM) results comparing key mechanical behaviors (Strength Capacity, Deflection, Slip Ratio, Initial and Ultimate Cracks, and Load-Strain) for SCTG and DCTG concrete specimens.

ACKNOWLEDGMENT

The authors would like to thank the Department of Civil Engineering at the Faculty of Engineering, Istanbul Gedik University, Istanbul, Türkiye, for their support.

REFERENCES

[1] Eurocode 4: Design of Composite Steel and Concrete Structures: General rule and rules for buildings, ENV1994-1-1: Part 1.1, European Committee for Standardization (CEN), Brussels, Belgium, 2004.

[2] Q. Zhang, S. Pei, Z. Cheng, Y. Bao, and Q. Li, "Theoretical and Experimental Studies of the Internal Force Transfer Mechanism of Perfobond Rib Shear Connector Group," *Journal of Bridge Engineering*, vol. 22, no. 2, Feb. 2017, Art. no. 04016112, https://doi.org/10.1061/(ASCE)BE.1943-5592.0000997.

[3] R. P. Johnson, Composite Structures of Steel and Concrete: Beams, Slabs, Columns, and Frames for Buildings, 3rd ed. Chichester: John Wiley & Sons, Incorporated, 2008.

[4] F. Wu, S. Liu, C. Xue, K. Yang, Y. Feng, and H. Zhang, "Experimental Study on the Mechanical Properties of Perfobond Rib Shear Connectors with Steel Fiber High Strength Concrete," *Materials*, vol. 14, no. 12, Jun. 2021, Art. no. 3345, https://doi.org/10.3390/ma14123345.

[5] P. Ansourian, "Experiments on Continuous Composite Beams," in *Institution of Civil Engineers, Proceedings, Pt2*, London, United Kingdom, Mar. 1983, vol. 73, pp. 25–51.

[6] W. Lin and T. Yoda, "Mechanical Behaviour of Composite Girders Subjected to Hogging Moment: Experimental Study," *Structural Engineering / Earthquake Engineering*, vol. 28, no. 2, pp. 29s–42s, 2011, https://doi.org/10.2208/jsceseee.28.29s.

[7] F. Alsharari, A. E.-D. El-Sisi, M. Mutnbak, H. Salim, and A. El-Zohairy, "Effect of the Progressive Failure of Shear Connectors on the Behavior of Steel-Reinforced Concrete Composite Girders," *Buildings*, vol. 12, no. 5, May 2022, Art. no. 596, https://doi.org/10.3390/buildings12050596.

[8] C. Wang, J. Xie, Y. Shen, and J. Jiang, "Research on the Mechanical Behavior of a Steel–Concrete Composite Link Slab on a Simply Supported Girder Bridge," *Metals*, vol. 12, no. 9, Aug. 2022, Art. no. 410, https://doi.org/10.3390/met12091410.

[9] C. Xue, Z. Fan, F. Wu, L. Liu, L. He, and X. Cui, "Research on the Shear Behaviour of Composite Shear Connectors," *Buildings*, vol. 12, no. 10, Oct. 2022, Art. no. 1726, https://doi.org/10.3390/buildings12101726.

[10] C. Lim, S.-H. Choi, J. Y. Oh, S.-J. Han, M.-S. Lee, and K. S. Kim, "Shear Behavior of Concrete Encased Steel Truss Composite Girders," *Applied Sciences*, vol. 11, no. 4, Feb. 2021, Art. no. 1569, https://doi.org/10.3390/app11041569.

[11] N. N. Long and N. X. Tung, "Analysis of a Steel-Concrete Composite Plate resting on Axial Bars using the Finite Element Method," *Engineering, Technology & Applied Science Research*, vol. 13, no. 4, pp. 11258–11262, Aug. 2023, https://doi.org/10.48084/etasr.6036.

[12] M. Hope Gill and R. Johnson, "Tests on Three Three-Span Continous Composit Beams.," *Proceedings of the Institution of Civil Engineers*, vol. 61, no. 2, pp. 367–381, Jun. 1976, https://doi.org/10.1680/iicep.1976.3445.

[13] Y. Liu, Z. Xiong, Y. Luo, G. Cheng, G. Liu, and J. Yang, "Double-composite rectangular truss bridge and its joint analysis," *Journal of Traffic and Transportation Engineering (English Edition)*, vol. 2, no. 4, pp. 249–257, Aug. 2015, https://doi.org/10.1016/j.jtte.2015.05.005.

[14] V. M. De Oliveira, A. S. De Carvalho, A. Rossi, F. P. V. Ferreira, and C. H. Martins, "Elastic and inelastic analyses of composite cellular beams in hogging moment regions," *Thin-Walled Structures*, vol. 184, Mar. 2023, Art. no. 110513, https://doi.org/10.1016/j.tws.2022.110513.

AUTHORS PROFILE

Jaafar J. Saleem is a structural bridge designer with B.Sc. and M.Sc. in civil engineering. His experience includes the State Commission for Roads and Bridges in Iraq. His research interests include steel and composite bridges. He has been involved in the design of several large bridges across various projects in Iraq.

Orcid ID 0009-0001-7677-1085.

Redvan Ghasemlounia is an Associate Professor and Head of the Department of Civil Engineering, Istanbul Gedik University and the Director of the Institute of Graduate Studies.

Orcid ID 0000-0003-1796-4562.

Haitham H. Muteb is a Professor in Structural Engineering with B.Sc., M.Sc., and Ph.D. degrees in Civil Engineering. His experience includes the Ministry of Higher Education and Scientific Research, the University of Babylon (College of Engineering and main campus), the University of Technology, Baghdad University, and the University of Karbala.

Orcid ID 0000-0002-4797-4561.